REPORT DOCUMENTATION PAGE

Form Approved
OMB No. 0704-0188

PLEASE DO NOT RETURN YOUR FORM TO THE ABOVE ORGANIZATION.

1. REPORT DATE *(DD-MM-YYYY)*	2. REPORT TYPE	3. DATES COVERED *(From - To)*
03-09-2009	Final	September 2007 - August 2009

4. TITLE AND SUBTITLE
Electric oxygen iodine laser: A study for scaling

5a. CONTRACT NUMBER

5b. GRANT NUMBER
FA9550-07-1-0529

5c. PROGRAM ELEMENT NUMBER

6. AUTHOR(S)
Michael C. Heaven

5d. PROJECT NUMBER

5e. TASK NUMBER

5f. WORK UNIT NUMBER

7. PERFORMING ORGANIZATION NAME(S) AND ADDRESS(ES)
Emory University, Department of Chemistry, 1515 Dickey Drive, Atlanta, GA 30322

8. PERFORMING ORGANIZATION REPORT NUMBER

9. SPONSORING/MONITORING AGENCY NAME(S) AND ADDRESS(ES)
AF Office of Scientific Research, 875 N. Randolph Street, Room 3112
Arlington, VA 22203

10. SPONSOR/MONITOR'S ACRONYM(S)
AFOSR

11. SPONSOR/MONITOR'S REPORT NUMBER(S)
AFRL-OSR-VA-TR-2012-0048

12. DISTRIBUTION/AVAILABILITY STATEMENT
Unlimited

13. SUPPLEMENTARY NOTES

14. ABSTRACT
Energy transfer reactions that could potentially limit scaling of the electric oxygen iodine laser (EOIL) were examined. Quenching of excited iodine atoms (I*) by atomic oxygen has been identified as a significant energy loss channel. The rate constant for this process was characterized over the temperature range from 295 to 360 K. Quenching of singlet oxygen (O2(a)) in moderate pressure discharges is a process that exhibits a non-linear pressure dependence. The reactions responsible for this behavior have been probed by examining the deactivation of O2(a) in the presence of O2(X) and O atoms. Rapid quenching was observed when both O2(X) and O were present, suggestive of a three-body process. However, a detailed kinetic analysis indicates that a reaction product (possibly vibrationally excited ozone) is the primary quenching agent. Detailed models of the post-discharge kinetics of EOIL were formulated and explored. The relative importance for various energy loss processes was evaluated, and weaknesses in the existing rate constant database were identified.

15. SUBJECT TERMS
Oxygen-iodine laser, discharge singlet oxygen generator, chemical kinetics, collisional energy transfer processes

16. SECURITY CLASSIFICATION OF:			17. LIMITATION OF ABSTRACT	18. NUMBER OF PAGES	19a. NAME OF RESPONSIBLE PERSON
a. REPORT	b. ABSTRACT	c. THIS PAGE			19b. TELEPHONE NUMBER *(Include area code)*
UU	UU	UU	UU		

Reset

Final technical report for the program

Electric oxygen iodine laser: A study for scaling

Grant number:	FA9550-07-1-0529
Period covered:	September 2007-August 2009
Performing organization:	Emory University, Atlanta GA
Principal Investigator:	Michael C. Heaven
Personnel:	Dr. Pavel Mikheyev (Senior visitor from the Lebedev Institute)
	Dr. Valeriy Azyazov (collaborator, Lebedev Institute)
	Ms. Marcia Gomes (graduate student)
	Mr. David Postel (graduate student)

Summary of accomplishments

Energy transfer reactions that could potentially limit scaling of the electric oxygen iodine laser (EOIL) were examined. Quenching of excited iodine atoms (I*) by atomic oxygen has been identified as a significant energy loss channel. The rate constant for this process was characterized over the temperature range from 295 to 360 K.

Quenching of singlet oxygen (O_2(a)) in moderate pressure discharges is a process that exhibits a non-linear pressure dependence. The reactions responsible for this behavior have been probed by examining the deactivation of O_2(a) in the presence of O_2(X) and O atoms. Rapid quenching was observed when both O_2(X) and O were present, suggestive of a three-body process. However, a detailed kinetic analysis indicates that a reaction product (possibly vibrationally excited ozone) is the primary quenching agent.

Detailed models of the post-discharge kinetics of EOIL were formulated and explored. The relative importance for various energy loss processes was evaluated, and weaknesses in the existing rate constant database were identified. An extended kinetic model of the iodine dissociation process was developed. This model is applicable to both electric and chemical oxygen iodine lasers.

Publications resulting from this research program:

V. N. Azyazov, P. A. Mikheyev, D. J. Postell and M. C. Heaven, Chem. Phys. Lett. Accepted, Sept 2009
"$O_2(a^1\Delta)$ quenching in the $O/O_2/O_3$ system"

P. A. Mikheyev, D. J. Postell and M. C. Heaven, J. App. Phys. 105 (2009) 094911
"Temperature dependence of the $O + I(^2P_{1/2}) \rightarrow O + I(^2P_{3/2})$ quenching rate constant"

V. N. Azyazov, S. Yu. Pichugin and M. C. Heaven, J. Chem. Phys. 130 (2009) 104306
"On the dissociation of I_2 by $O_2(a^1\Delta)$: Pathways involving the excited species $I_2(A'^3\Pi_{2u}$, $A^3\Pi_{1u})$, $I_2(X^1\Sigma, \upsilon)$ and $O_2(a^1\Delta, \upsilon)$"

V. N. Azyazov, S. Yu. Pichugin and M. C. Heaven, Proc. SPIE, vol. 7131, paper 22 (2008)
"Multi-pathway I_2 dissociation model for COIL"

1. Temperature dependence of the $O + I(^2P_{1/2}) \rightarrow O + I(^2P_{3/2})$ quenching rate constant

Discharge singlet oxygen generators add complexity to the chemistry of the oxygen iodine laser as oxygen atoms are not produced in the chemically driven system. The oxygen atoms in the post discharge flow were shown to effect the performance of the laser to such a great extent that removal of the oxygen was required in order to achieve gain on the I*-I transition [1-4]. Removal was accomplished by addition of NO_2 to the flow. Several previous studies have addressed the collisional deactivation of I* by ground state oxygen atoms [1-4].

$$I^*(^2P_{1/2}) + O(^3P) \rightarrow I(^2P_{3/2}) + O(^3P)$$

Kinetic measurements that were designed to isolate the quenching reaction were conducted at room temperature [5,6]. An additional complication that arises with use of the discharge is that the excess energy goes into heating of the post-discharge flow. Experiments and modeling of the discharge driven laser indicate temperatures well above 350 K for most conditions. Prior to the work reported here, no systematic studies of the temperature dependence of this rate coefficient had been made. The value given by the recent room temperature studies seems to aid in modeling of EOIL, but measurements of this rate coefficient at elevated temperatures were needed. In addition, temperature dependent studies also help determine the validity of the previous hypothesis that the quenching process occurs via a curve crossing mechanism.

The rate constant for quenching of $I(^2P_{1/2})$ by $O(^3P)$ was been measured for the temperature range 295-360K. Pulsed laser photolysis of mixtures N_2O and I_2 was used to examine the kinetics. $O(^3P)$ atoms were produced by the photo-initiated reaction sequence $N_2O+h\nu \rightarrow O(^1D)+N_2$, $O(^1D)+M \rightarrow O(^3P)+M$, while singlet oxygen was generated by the secondary reaction $O(^1D)+N_2O \rightarrow O_2(a^1\Delta)+N_2$. Iodine atoms were produced by I_2 photodissociation and from the secondary reactions of I_2 with $O(^3P)$ atoms. Subsequent excitation of I by $O_2(a^1\Delta)$ led to $I(^2P_{1/2})$ formation, with $I(^2P_{1/2})$ concentrations monitored using time-resolved 1315 nm emission. The rate constant of the quenching process was determined by fitting a kinetic model to the observed emission traces. Special attention was given to the gas flow conditions.

A modest temperature dependence of the quenching rate constant was found, and this was well represented by the equation $k = (6.5\pm1.0)\times10^{-12}(T/300)^{1.76}$ cm^3s^{-1}. The room temperature rate constant differs from previous experimental determinations. The temperature dependent rate constant agrees well with the value obtained by computational modeling of the data from discharge-driven oxygen iodine lasers at a nominal temperature of 375 K.

2. Quenching of $O_2(a)$ in the presence of O and O_2

The maximum $O_2(a^1\Delta)$ yields in discharge systems obtained so far (15-20 %) have been for relatively low oxygen pressures. In this case the concentration of the active components in the flow is small, resulting in a low gain coefficient. To produce a high-power oxygen iodine laser system it will be necessary to significantly increase the

operating pressure of the device. Braginskiy et al. [7] observed that the $O_2(a^1\Delta)$ yield at the exit of discharge singlet oxygen generator decreased with increasing oxygen pressure. They suggested that faster deactivation of singlet oxygen was encountered at higher pressures due to the three-body quenching process.

$$O(^3P) + O_2(a^1\Delta) + O_2 \rightarrow O(^3P) + O_2 + O_2$$

If this is correct, the pressure scaling of $O_2(a^1\Delta)$ densities will be limited by three-body quenching if the production of O atoms is not adequately controlled. To explain the singlet oxygen dynamics in the post-discharge flow, Braginskiy et al. [7] proposed that the rate constant for the three-body deactivation was in the range $k_{3b} = (1\text{-}3)\times10^{-32}$ cm^6/s.

In the present work, 248 nm laser photolysis of $O_3/O_2/Ar/CO_2$ mixtures was employed to study the kinetics of $O_2(a^1\Delta)$ in the presence of oxygen atoms, O_2 and ozone. UV photolysis of ozone yields the products:

$$\begin{aligned} O_3 + h\nu \quad &\rightarrow O(^1D) + O_2(a^1\Delta) \\ &\rightarrow O(^3P) + O_2(X^3\Sigma), \end{aligned}$$

where the singlet oxygen yield is 90 %. The $O_2(a^1\Delta)$ removal rate was monitored by observing the time evolution of the O_2 emission at a wavelength of λ=1268 nm. The temporal profiles of the oxygen atom concentrations were monitored by means of the O+NO+M chemiluminescent reaction.

Fast and slow decays of $O_2(a^1\Delta)$ were observed. The fast decay was observed when O atoms were present in the system. An attempt was made to model the fast decay using the three body quenching process $O_2(a^1\Delta) + O + O_2 \rightarrow 2O_2 + O$ suggested by Braginskiy et al. [7] The near gas kinetic rate constant obtained from this analysis ($(1.1\pm0.1)\times10^{-31}$ cm^6/s) was inconsistent with data obtained from flowing afterglow experiments, indicating that additional quenching species are generated by the ozone photochemistry. Rate constants for quenching of $O_2(b^1\Sigma)$ by CO_2 ($(6.1\pm0.5)\times10^{-13}$ cm^3/s) and O_3 ($(1.9\pm0.2)\times10^{-11}$ cm^3/s) were measured as a test of the kinetic analysis techniques.

3. Post discharge kinetics in $He/O_2/NO/I_2$ mixtures

The relative importance of various known reactions in the flowing afterglow of electrically discharged $He/O_2/NO/I_2$ mixtures was evaluated for the experimental conditions and the model described by Palla et al. [1]. The results and modeling of references were also taken into account. Other rate constants were taken from references[8-12]. A kinetic model based on most of the reactions that could be found in literature was developed and rates of the reactions were compared straightforwardly to determine which are most important. The gas temperature after the discharge was assumed to be 415 °K as that value provided a good agreement with [O] concentrations obtained by modeling in reference [1]. The transport time from the discharge exit to the point where NO_2 was injected was derived from the data in [1] and assumed to be 30 ms. The temperature at this point was assumed to be 375 °K. Then, after a further 10 ms of transport time, I_2 was injected at 360 °K. The reactions were monitored for another 10 ms, until I_2 dissociation was complete. In the EOIL device modeled, Ar or N_2 was injected, prior to a supersonic expansion [1]. After that point the concentrations of O_2 and I* were reduced by a factor of about three, considerably reducing the quenching rates.

Reactions considered in the model are listed in table 1.

Table1.

k	Reaction							Rate constant ($cm^3(cm^6)s^{-1}$)	Ref
1	$O_2(^1\Delta)$	+	$O_2(^1\Delta)$	→	$O_2(^1\Sigma)$	+	O_2	$9.8\times10^{-28}T^{3.8}\exp(700/T)$ $9\times10^{-17}\exp(-560/T)$ 2.7×10^{-17}	[1,5,6] [13] [14]
2	$O_2(^1\Delta)$	+	$O_2(^1\Delta)$	→	O_2	+	O_2	1.7×10^{-17} $9\times10^{-17}\exp(-560/T)$	[1,13]
3	$O_2(^1\Delta)$	+	NO	→	NO	+	O_2	8.5×10^{-17}	[15]
4	$O_2(^1\Delta)$	+	O_2+O	→	O_2+ O_2	+	O	1.0×10^{-32} 2.5×10^{-32}	[1,15,16]
5	$O_2(^1\Delta)$	+	O_2	→	O_2	+	O_2	8.2×10^{-19} $(1.58\text{-}2.2)\times10^{-18}(T/300)^{0.8}$ $3\times10^{-18}\exp(-200/T)$	[1] [7]
6	$O_2(^1\Delta)$	+	O	→	O_2	+	O	7×10^{-16} 2×10^{-16}	[1,7]
7	2O	+	O	→	$O_2(^1\Delta)$	+	O	$6.93\times10^{-35}(T/300)^{-0.63}$	[13]
8	2O	+	O_2	→	$O_2(^1\Delta)$	+	O	$1.93\times10^{-35}(T/300)^{-0.63}$ $3.8\times10^{-31}\times T^{-1}\exp(-170/T)$	[1,13]
9	2O	+	$O_2(^1\Delta)$	→	$O_2(^1\Delta)$	+	O_2	$4.5\times10^{-34}\exp(630/T)$	[1]
10	2O	+	He	→	$O_2(^1\Delta)$	+	He	9.88×10^{-35}	[13]
11	2O	+	O	→	O_2	+	O	$9.21\times10^{-34}(T/300)^{-0.63}$ $4.5\times10^{-34}\exp(630/T)$	[1,12,13]

12	2O	+	O_2	→	O_2	+	O_2	$2.56\times10^{-34}(T/300)^{-0.63}$ $4.5\times10^{-34}\exp(630/T)$ $3.34\times10^{-30}\times T^{-1}\exp(-170/T)$	[1,7, 13]
13	2O	+	He	→	O_2	+	He	1×10^{-33} $4.5\times10^{-34}\exp(630/T)$	[1,13]
14	O	+	O_2 +He	→	O_3	+	He	$5.1\times10^{-27}T^{-2.8}$ $3.4\times10^{-34}(T/300)^{-1.2}$	[1,13]
15	O	+	$2O_2$	→	O_3	+	O_2	$5.1\times10^{-27}T^{-2.8}$ $6.2\times10^{-34}(T/300)^{-2.}$	[1,7]
16	2O	+	O_2	→	O_3	+	O	$4.5\times10^{-34}\exp(630/T)$ $2.5\times10^{-34}\exp(345/T)$	[1,7]
17	O	+	$O_2 + O_2(^1\Delta)$	→	$O_2(^1\Delta)$	+	O_3	$5.1\times10^{-27}T^{-2.8}$	[1]
18	O_3	+	$O_2(^1\Delta)$	→	$2O_2$	+	O	$5.2\times10^{-11}\exp(-2840/T)$	[12]
19	O_3	+	O	→	$O_2(^1\Delta)$	+	O_2	$2.4\times10^{-13}\exp(-2060/T)$ $2.0\times10^{-11}\exp(-2280/T)$ $1.0\times10^{-11}\exp(-2300/T)$	[7] [8]
20	O_3	+	O	→	O_2	+	O_2	$8\times10^{-12}\exp(-2060/T)$	[7,13]
21	O_3	+	O	→	$O_2(^1\Sigma)$	+	O	$8\times10^{-14}\exp(-2060/T)$	[15]
22	O	+	$NO+O_2$	→	NO_2	+	O_2	$4.68\times10^{-28}T^{-1.5}$	[1]
23	O	+	NO+He	→	NO_2	+	He	$2.08\times10^{-28}T^{-1.5}$	[1]
24	O	+	NO_2	→	NO	+	O_2	$6.5\times10^{-12}\exp(120/T)$ 9.7×10^{-12}	[1] [15]
25	NO	+	O_3	→	NO_2	+	O_2	$1.4\times10^{-12}\exp(-1310/T)$	[12]
26	$O_2(^1\Sigma)$	+	O	→	$O_2(^1\Delta)$	+	O	7.2×10^{-14} $7.2\times10^{-14}\times(T/300)^{0.5}$	[12,13]
27	$O_2(^1\Sigma)$	+	O	→	O_2	+	O	8×10^{-15} $8\times10^{-15}\times(T/300)^{0.5}$ 1.5×10^{-16}	[1] [13] [7]
28	$O_2(^1\Sigma)$	+	O_3	→	$2O_2$	+	O	$7.33\times10^{-12}(T/300)^{0.5}$ 1.5×10^{-11}	[1,7, 13] [8]
29	$O_2(^1\Sigma)$	+	O_3	→	$O_2(^1\Delta)$	+	O_3	$7.33\times10^{-12}(T/300)^{0.5}$ 7.1×10^{-12} 3.3×10^{-12}	[1,7, 13]
30	$O_2(^1\Sigma)$	+	O_3	→	O_2	+	O_3	$7.33\times10^{-12}(T/300)^{0.5}$ 3.3×10^{-12}	[7,13] [1]
31	$O_2(^1\Sigma)$	+	O_2	→	$O_2(^1\Delta)$	+	O_2	$3.6\times10^{-17}(T/300)^{0.5}$ 3.710^{-17}	[1,13]
32	$O_2(^1\Sigma)$	+	O_2	→	O_2	+	O_2	$4\times10^{-18}\times(T/300)^{0.5}$ 1.5×10^{-16} $4.3\times10^{-22}\times T^{-2.4}\exp(-241/T)$	[7,13] [11]
33	2O	+	O_2	→	$O_2(^1\Sigma)$	+	O_2	$7.6\times10^{-32}\times T^{-1}\exp(-170/T)$	[7]
34	I_2	+	O	→	IO	+	I	1.25×10^{-10}	[12]
35	IO	+	O	→	O_2	+	I	1.4×10^{-10}	[12]
36	IO	+	IO	→	O_2	+	I_2	$5.4\times10^{-11}\exp(180/T)$	[12]

37	I	+	$O_2(^1\Delta)$	→	I*	+	O_2	$2.3\times10^{-8}/T$	[1]
38	I*	+	O_2	→	$O_2(^1\Delta)$	+	I	$3.1\times10^{-8}\times T^{-1}\exp(-403/T)$	[1]
39	I*	+	NO	→	NO	+	I	1.2×10^{-13}	[1]
40	I*	+	I_2	→	I_2*	+	I	3.8×10^{-11} $1.4\times10^{-13}\exp(1600/T)$	[1,14]
41	I*	+	I	→	I	+	I	1.7×10^{-13} 1.6×10^{-14}	[1] [14]
42	I	+	NO+M	→	INO	+	M	1.8×10^{-33}	[12]
43	I	+	INO	→	NO	+	I_2	2.6×10^{-10}	[10]
44	I*	+	$O_2(^1\Delta)$	→	$O_2(^1\Sigma)$	+	I	1.1×10^{-13} $4\times10^{-24}\times T^{-3.8}\times\exp(700/T)$	[1,14]
45	I*	+	$O_2(^1\Delta)$	→	$O_2(^1\Delta)$	+	I	1.1×10^{-13}	[1]
46	I*	+	O	→	O	+	I	$6.5\times10^{-12}\times(T/300)^{1.76}$ 8×10^{-12}	[1]
47	I_2*	+	$O_2(^1\Delta)$	→	O_2	+	2I	3×10^{-10}	[14]
48	I_2*	+	O_2	→	O_2	+	I_2	4.9×10^{-12}	[1]
49	$O_2(^1\Sigma)$	+	I_2	→	O_2	+	2I	3.8×10^{-11} 4×10^{-12}	[1] [14]
50	$O_2(^1\Sigma)$	+	I_2	→	$O_2(^1\Delta)$	+	I_2	2.3×10^{-11}	[1]
51	$O_2(^1\Sigma)$	+	NO	→	$O_2(^1\Delta)$	+	NO	6.0×10^{-14}	[1] [15]
52	$O_2(^1\Sigma)$	+	He	→	$O_2(^1\Delta)$	+	He	1.0×10^{-17}	[1]
53	$O_2(^1\Delta)$	+	wall	→	O_2			$3\times10^{-5}\times\langle v\rangle/2R$	[15]
54	O	+	wall	→	$^1/_2O_2$			$4\times10^{-4}\times\langle v\rangle/2R$ $(1\text{-}3)\times10^{-3}\times\langle v\rangle/2R$	[7,17]
55	$O_2(^1\Sigma)$	+	wall	→	O_2			$1\times10^{-2}\times\langle v\rangle/2R$	[18]

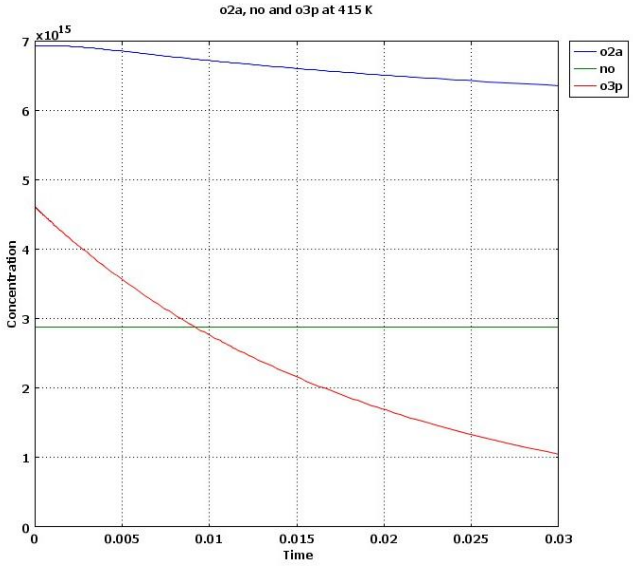

Figure 1. Evolution of O_2(a), NO and O(^{3}P) during 30 ms transport.

The kinetics for different species were analyzed separately to understand the importance of reaction rates that cause their production and removal during specified time intervals. $O_2(a^1\Delta)$, $O_2(b^1\Sigma)$, O_3, O, I*, I, NO, NO_2 and O_2 are denoted in the figures as o2a, o2b, o3, o3p, iex, ix, no, no2 and o2x .

Initial values for the concentrations right after the discharge were chosen to be close to those given in [1]. Specifically, $[O_2]=4.8\times10^{16}$, $[O_2(^1\Delta)]=6.9\times10^{15}$, $[O_2(^1\Sigma)]=6.9\times10^{14}$, $[O_3]=0$, $[O]=4.8\times10^{15}$, and $[NO]=2.9\times10^{15}$ cm^{-3} at 415 °K.

The evolution of $[O_2(^1\Delta)]$, [O] and [NO] during the 30 ms transport is represented in Figure 1. The number densities for this group are of the same order of magnitude (10^{15} cm^{-3}) during first 30 ms of transportation. NO added to the discharge favors singlet oxygen production [1,15] and provides the fastest channel of O atom removal in the reaction sequence 22-24. O_3, NO_2 and $O_2(^1\Sigma)$ are also present in the gas stream from the dischsrge. These species have number densities two orders of magnitude lower than those of Fig. 1. The evolution for this second group during transport is shown in Fig. 2.

Singlet delta oxygen.

The rates for quenching of $O_2(^1\Delta)$ are represented in Fig. 3. The reactions are listed in the caption according to their rates in descending order. They are reactions 4, 18, 6, 1, 3, 53, 2, 5 in Table 1. Rates 2 and 5 contribute just 13 % of the quenching, and only at the end of 30 ms time interval. Hence, these reactions may be neglected at shorter times. Although $[O_3]$ is quite low its contribution to $O_2(^1\Delta)$ quenching is one of the largest. It should be noted that the rate constants of the most important reactions 4 and 6 are known poorly and different authors use quite different values, as seen from the table.

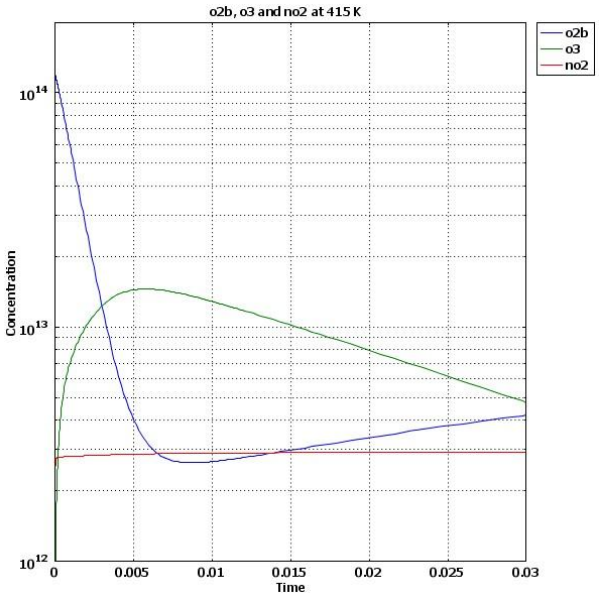

Figure 2. Evolution of O_2(b), NO_2 and O_3 during 30 ms transport.

Wall recombination was considered in refs [15,17]. The rate coefficient for this reaction is estimated by $k_w=\gamma\langle v\rangle/2R$, where $\gamma=3\times10^{-5}$ [15] is the recombination probability, $\langle v\rangle\approx3\times10^4$ cm/s is the mean oxygen atom thermal velocity, and 2R=5 cm is the tube diameter [1]. As can be seen in Fig. 3, wall recombination should be taken into account on this time scale because at the beginning its contribution is 5% and at the end it has increased to 20%.

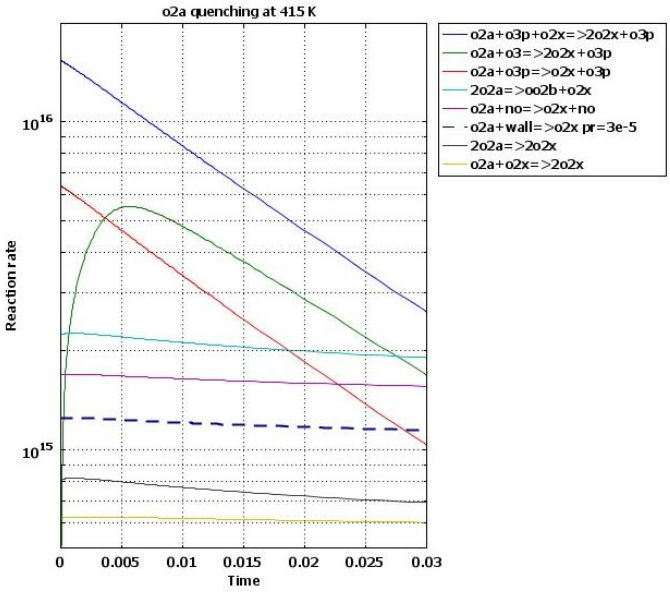

Figure 3. O_2(a) quenching rates.

Some $O_2(^1\Delta)$ is produced in the afterglow, mostly due to $O_2(^1\Sigma)$ conversion, resulting in a small rise of $[O_2(^1\Delta)]$ right after discharge. Rates for the reactions 7, 8, and 31 are smaller than 3×10^{14} $cm^{-3}s^{-1}$ and may be safely excluded from the model as their contribution to $O_2(^1\Delta)$ production is less than 3%. Different authors [7,8,18] use rate coefficients for reaction 19 with 2 orders of magnitude difference. If the largest estimate is correct, this reaction should be taken into account.

For the experimental conditions of [1] the overall loss of $O_2(^1\Delta)$ during first 30 ms after discharge is about 7%. This figure remains the same regardless of the presence or absence of NO in the system. The reason is that in the absence of NO, despite a larger quenching by O, some $O_2(^1\Delta)$ is produced by reaction 10. However, for the higher yield of $[O_2(^1\Delta)]$ obtained in [15] and with O atoms removed by HgO in the discharge, the presence of NO facilitates $O_2(^1\Delta)$ quenching.

Oxygen atoms

In the presence of NO the fastest rates of O atoms removal are from reactions 24, 23, 22, 53, 13, 14, 12, and 15. The reaction rates are in the range 10^{15}-10^{17} $cm^{-3}s^{-1}$. It is important to note that the next largest removal rate is provided by wall recombination with $\gamma=4\times10^{-4}$ [17] which must be accounted for in the modeling. In the absence of NO the rate of heterogeneous recombination dominates. Reactions 18, 20, 16, and 10, with rates are in the range $(0.1\text{-}5)\times10^{15}$ $cm^{-3}s^{-1}$ are also important for modeling, as they determine [O] in the absence of NO.

The rates of reactions 7-9, 11, 19, 21 are less than 2×10^{14} $cm^{-3}s^{-1}$ and their sum is less than 5×10^{14} $cm^{-3}s^{-1}$. Consequently, they may be excluded from the model (bearing in mind the problem with the rate constant for reaction 19) as their contribution to the total [O] removal is about 1%.

$O_2(^1\Sigma)$ and O_3

In the absence of iodine, $O_2(^1\Sigma)$ is produced in reactions 1 (pooling) and 33. The latter contributes less than 5% and may be safely discarded. Removal of $O_2(^1\Sigma)$ occurs via reactions 26, 51, 28, 55, 27, 29, 30 corresponding to their descending rates and the order they appear in Fig. 4. Reactions 31, 32, 52 may be neglected, being two orders of magnitude slower. After the removal of most of the O atoms, quenching of $O_2(^1\Sigma)$ by NO and wall collisions ($\gamma=1\times10^{-2}$) [18] are the dominant removal pathways.

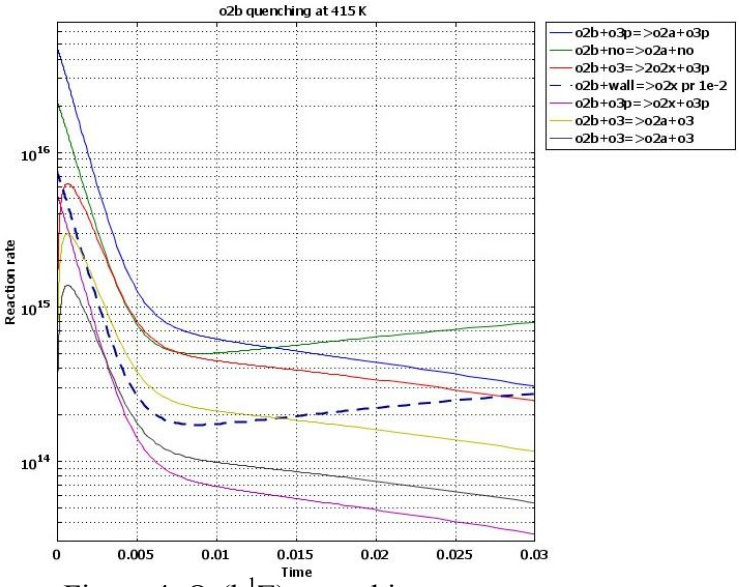

Figure 4. $O_2(b^1\Sigma)$ quenching rates.

The concentration of ozone generated by the discharge is small [1,13]. Ozone production in the afterglow occurs via reactions 14-17 and it is removed by reactions 25, 18, 19, and 28. Reactions 17 and 19 contribute less then 3% to the rate and may be discarded. After a brief increase, $[O_3]$ decreases during transport, and after 30 ms drops to $\approx5\times10^{12}$ cm^{-3} (Fig. 2).

Behavior of the system after NO_2 and I_2 injection

After NO_2 injection the O atoms are rapidly eliminated from the system and slow $O_2(^1\Delta)$ quenching occurs due to reactions 3 (NO quenching), 1 (pooling), 53 (wall), 2 (self quenching) and 5 (by O_2) resulting in less than 2% decrease in $[O_2(^1\Delta)]$ during 10 ms before I_2 is injected.

After I_2 injection, the loss of $O_2(^1\Delta)$ substantially increases due to I* quenching reactions. Fig. 5 shows that I_2 dissociation is complete after 10 ms. Details of the I_2 dissociation mechanism are not considered here and the process is treated empirically using reactions 40 and 47.

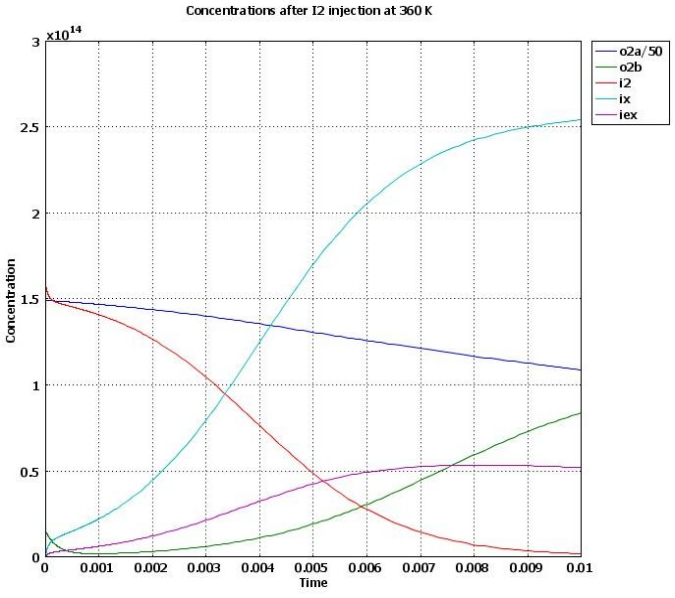

Figure 5. Concentrations after I_2 injection. $[O_2(^1\Delta)]$ is scaled to fit the figure.

Experiments and modeling [1] have shown that lasing can be

achieved only when most of the O atoms are removed from the system. The present calculations indicate that the dissociation of I_2 proceeds without significant contributions from reactions 34 and 35. Even at a low level, the presence of O atoms decreases $[O_2(^1\Delta)]$ during I_2 dissociation.

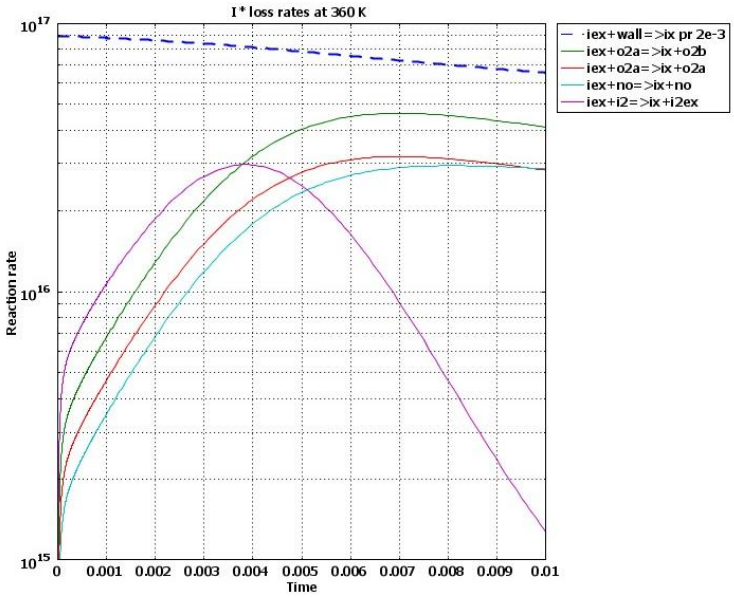

Figure 6. Loss rates after I_2 injection.

Rates of I* loss are depicted in Fig. 6. Reactions I*+wall, 44, 45, 39, 40 correspond to the rates in decreasing order. As there is a near equilibrium between $O_2(^1\Delta)$, O_2, I and I*, irreversible loss of I* is equivalent to loss of $O_2(^1\Delta)$. This makes wall quenching of I* an important process. This situation was considered in detail in reference [19], and it was found that, for the typical conditions of a chemical oxygen-iodine laser, wall loss may be assessed by assigning a wall loss probability for $O_2(^1\Delta)$ of the order $[I]/[O_2]$, assuming that every I*+wall collision results in deactivation. With the increase of [I] during I_2 dissociation this value changes and under the conditions of reference [1] the mean estimated wall loss probability is 2×10^{-3}. Fig. 6 shows this to be the dominant loss process after I_2 addition.

The rate constant of reaction 41 used in [1] is an order of magnitude larger than in [14], but its rate is, nevertheless low and it may be disregarded. The rate of NO assisted I recombination due to reactions 42, 43 is smaller than rate of reaction 41 and may also be neglected. In the absence of O atoms reaction 46 does not contribute to I* quenching.

Conclusions

Of the reactions listed in Table 1, 15 have been identified that are not of importance in modeling EOIL systems. These are reactions 7-9, 11, 17, 19, 21, 31-33, 41-43, 52. The rate coefficient of reaction 19 differs by two orders of magnitude in the literature. If the true value is close to the upper limit, reaction 19 should remain in the model. Heterogeneous quenching is identified as being important in the post discharge kinetics.

4. On the dissociation of I_2 by $O_2(a^1\Delta)$: Pathways involving the excited species $I_2(A'^3\Pi_{2u}, A^3\Pi_{1u})$, $I_2(X^1\Sigma, \upsilon)$ and $O_2(a^1\Delta, \upsilon)$

Kinetic studies were carried out to explore the role of the excited species $I_2(A'^3\Pi_{2u}, A^3\Pi_{1u})$, $I_2(X^1\Sigma, \upsilon)$ and $O_2(a^1\Delta, \upsilon)$ in the dissociation of I_2 by singlet oxygen. A flow tube apparatus that utilized a chemical singlet oxygen generator was used to measure the I_2 dissociation rate in $O_2(a^1\Delta)/I_2$ mixtures. Vibrationally excited $I_2(X)$ is thought to be a significant intermediate in the dissociation process. Excitation probabilities (γ_υ) for population of the υ-th $I_2(X)$ vibrational level in the reaction $I_2(X)+I(^2P_{1/2}) \rightarrow I_2(X, \upsilon>10)+I(^2P_{3/2})$ were estimated based on a comparison of calculated populations with experimentally determined values. Satisfactory agreement with the experimental data was achieved for total excitation probabilities partitioned in two ranges, such that $\Gamma_{25\le\upsilon\le47} = \sum_{\upsilon=25}^{47}\gamma_\upsilon \approx 0.1$ and $\Gamma_{15\le\upsilon\le23} = \sum_{\upsilon=15}^{23}\gamma_\upsilon \approx 0.9$. A multi-pathway I_2 dissociation model was developed in which the intermediates are $I_2(A'^3\Pi_{2u}, A^3\Pi_{1u})$ and $I_2(X,\upsilon)$. It was shown that the iodine dissociation process passes predominantly through the $I_2(A'^3\Pi_{2u}, A^3\Pi_{1u})$ intermediate. These states are populated mainly by collisions of I_2 with vibrationally excited $O_2(a^1\Delta, \upsilon)$ when the mole fraction of I_2 is small (η_{I_2}<1%), and by collisions of $I_2(X,15\le\upsilon\le23)$ with $O_2(a^1\Delta)$ for higher concentrations (η_{I_2}>1%). The revised kinetic model is defined below in Table 4.1

Table 4.1. The extended kinetics model for COIL

#	Reaction	Rate constant (T=300 K), cm^3/s
1	$O_2(a) + O_2(a) \rightarrow O_2(b) + O_2(X)$	2.5×10^{-17}
2	$O_2(a) + O_2(a) \rightarrow O_2(a) + O_2(X)$	0
3	$O_2(a) + O_2(a) \rightarrow O_2(X) + O_2(X)$	1.7×10^{-17}
4	$O_2(b) + O_2(X) \rightarrow O_2(a) + O_2(X)$	3.9×10^{-17}
5	$O_2(b) + H_2O \rightarrow O_2(a, \upsilon) + H_2O$	6.7×10^{-12}
6	$O_2(b) + Cl_2 \rightarrow O_2(a) + Cl_2$	2.0×10^{-15}
7	$O_2(b) + H_2O_2 \rightarrow O_2(a) + H_2O_2$	3.3×10^{-13}
8	$O_2(b) + He \rightarrow O_2(a) + He$	1.0×10^{-17}
9	$O_2(b) + CO_2 \rightarrow O_2(a, \upsilon) + CO_2$	6×10^{-13}
14	$O_2(a) + O_2(X) \rightarrow O_2(X) + O_2(X)$	1.6×10^{-18}
15	$O_2(a) + H_2O \rightarrow O_2(X) + H_2O$	4.0×10^{-18}
16	$O_2(a) + Cl_2 \rightarrow O_2(X) + Cl_2$	6.0×10^{-18}
17	$O_2(a) + H_2O_2 \rightarrow O_2(X) + H_2O_2$	0
18	$O_2(a) + He \rightarrow O_2(X) + He$	8.0×10^{-21}
21	$I_2(X) + O_2(b) \rightarrow I + I + O_2(X)$	3.3×10^{-11}
22	$I_2(X) + O_2(b) \rightarrow I_2(X) + O_2(a)$	2.5×10^{-11}
24	$I_2(X) + O_2(b) \rightarrow I_2(A,A') + O_2(X)$	0
25	$I_2(A,A') + O_2(a) \rightarrow I + I + O_2(X)$	3×10^{-11}
26	$I_2(A,A') + O_2(a) \rightarrow I_2(B) + O_2(X)$	$<10^{-12}$
27	$I_2(B) + O_2 \rightarrow I + I + O_2$	6×10^{-11}
28	$I_2(A') + O_2(X) \rightarrow I_2(X) + O_2(a)$	6.3×10^{-12}
29.1	$I_2(A') + H_2O \rightarrow I_2 + H_2O$	3.4×10^{-12}
29.2	$I_2(A') + N_2 \rightarrow 2I + N_2$	3.5×10^{-14}
29.3	$I_2(A') + CO_2 \rightarrow I_2 + CO_2$	8.5×10^{-13}
29.4	$I_2(A') + He \rightarrow 2I + He$	9.4×10^{-15}
30	$I_2(B) \rightarrow I + I$	$6\times10^{5}\ s^{-1}$
31	$I_2(B) \rightarrow I_2(X) + h\nu$	$6\times10^{5}\ s^{-1}$
32	$I_2(X) + O_2(a) \rightarrow I_2(X,\upsilon) + O_2(X)$	$<5.0\times10^{-16}$
33	$I_2(X) + I^* \rightarrow I_2(X,\upsilon>10) + I$	3.8×10^{-11}
34	$I_2(X,\upsilon\geq25) + O_2(a) \rightarrow I + I + O_2(X)$	3×10^{-11}
35	$I_2(X,\upsilon) + O_2 \rightarrow I_2(X,\upsilon\text{-}1) + O_2$	$\upsilon\times2.7\times10^{-12}$
36	$I_2(X,\upsilon) + H_2O \rightarrow I_2(X,\upsilon\text{-}1) + H_2O$	$\upsilon\times6\times10^{-12}$
37	$I_2(X,\upsilon) + He \rightarrow I_2(X,\upsilon\text{-}1) + He$	$\upsilon\times3.9\times10^{-12}$
38	$I_2(X,\upsilon) + N_2 \rightarrow I_2(X,\upsilon\text{-}1) + N_2$	$\upsilon\times3.4\times10^{-12}$
39	$I_2(X,\upsilon) + CO_2 \rightarrow I_2(X,\upsilon\text{-}1) + CO_2$	$\upsilon\times3.4\times10^{-12}$
40	$I + O_2(a) \rightarrow I^* + O_2(X)$	7.8×10^{-11}
41	$I^* + O_2(X) \rightarrow I + O_2(a)$	2.7×10^{-11}
42	$I + O_2(a) \rightarrow I + O_2(X)$	1.0×10^{-15}
43	$I^* + O_2(X) \rightarrow I + O_2(X)$	0
44	$I^* + O_2(a) \rightarrow I + O_2(b)$	1.1×10^{-13}
45	$I^* + O_2(a) \rightarrow I + O_2(a)$	1.1×10^{-13}

46	$I^* + O_2(a) \rightarrow I + O_2(X)$	0
47	$I^* + I \rightarrow I + I$	1.6×10^{-14}
48	$I^* + H_2O \rightarrow I + H_2O$	2.0×10^{-12}
49	$I^* + H_2O_2 \rightarrow I + H_2O_2$	2.5×10^{-11}
50	$I^* + He \rightarrow I + He$	5.0×10^{-18}
51	$I^* + O_2(X) \rightarrow I + O_2(X)$	3.5×10^{-16}
53	$I^* \rightarrow I + h\nu$	7.8 s^{-1}
54	$I^* + Cl_2 \rightarrow ICl + Cl$	5.5×10^{-15}
56	$I^* + ICl \rightarrow I_2 + Cl$	1.5×10^{-11}
57	$I_2 + Cl \rightarrow ICl + I$	2.0×10^{-10}
58	$ICl + Cl \rightarrow Cl_2 + I$	8.0×10^{-12}
59	$I + I + I_2(X) \rightarrow I_2(X) + I_2(X)$	3.6×10^{-30} cm^6/s
60	$I^* + I + I_2(X) \rightarrow I_2(B) + I_2(X)$	$<3.6\times10^{-30}$ cm^6/s
61	$I + I + He \rightarrow I_2(X) + He$	3.6×10^{-33} cm^6/s
62	$I + I + O_2(X) \rightarrow I_2(X) + O_2(X)$	3.7×10^{-32} cm^6/s
70	$O_2(\upsilon) + O_2 \rightarrow O_2(\upsilon\text{-}1) + O_2$	8.2×10^{-19}
71	$O_2(\upsilon) + H_2O \rightarrow O_2(\upsilon\text{-}1) + H_2O$	8.2×10^{-17}
72	$O_2(\upsilon) + He \rightarrow O_2(\upsilon\text{-}1) + He$	0
73	$O_2(\upsilon) + N_2 \rightarrow O_2(\upsilon\text{-}1) + N_2$	0
76	$O_2(X,2) + O_2(X,0) \rightarrow O_2(X,1) + O_2(X,1)$[a]	2.0×10^{-13}
77	$O_2(X,3) + O_2(X,0) \rightarrow O_2(X,2) + O_2(X,1)$	2.6×10^{-13}
78	$O_2(X,4) + O_2(X,0) \rightarrow O_2(X,3) + O_2(X,1)$	2.7×10^{-13}
79	$O_2(a,1) + CO_2 \rightarrow O_2(a,0) + CO_2(\upsilon)$	1.8×10^{-14}
80	$O_2(a,2) + CO_2 \rightarrow O_2(a,1) + CO_2(\upsilon)$	4.4×10^{-14}
81	$O_2(a,3) + CO_2 \rightarrow O_2(a,2) + CO_2(\upsilon)$	1.0×10^{-13}
82	$O_2(b,1) + CO_2 \rightarrow O_2(b,0) + CO_2(\upsilon)$	1.2×10^{-12}
83	$O_2(b,2) + CO_2 \rightarrow O_2(b,1) + CO_2(\upsilon)$	1.7×10^{-12}
84	$O_2(b,3) + CO_2 \rightarrow O_2(b,2) + CO_2(\upsilon)$	1.6×10^{-12}
85	$O_2(X,1) + H_2O(000) \rightarrow O_2(X,0) + H_2O(010)$	1.7×10^{-12}
89	$O_2(a,1) + O_2(X,0) \rightarrow O_2(X,1) + O_2(a,0)$	5.6×10^{-11}
90	$O_2(a,2) + O_2(X,0) \rightarrow O_2(X,2) + O_2(a,0)$	3.6×10^{-11}
91	$O_2(b,1) + O_2(X,0) \rightarrow O_2(X,1) + O_2(b,0)$	1.52×10^{-11}
92	$O_2(b,2) + O_2(X,0) \rightarrow O_2(X,2) + O_2(b,0)$	1.7×10^{-12}
93	$O_2(b,3) + O_2(X,0) \rightarrow O_2(X,3) + O_2(b,0)$	1.5×10^{-13}
94	$H_2O(010) + H_2O \rightarrow H_2O(000) + H_2O$	5×10^{-11}
95	$O_2(a,1) + I_2(X) \rightarrow O_2(X) + I_2(A')$	2×10^{-12}
96	$O_2(a,2) + I_2(X) \rightarrow O_2(X) + I_2(A)$	3×10^{-11}
97	$O_2(a,3) + I_2(X) \rightarrow O_2(X) + 2I$	10^{-11}
101	$O_2(a) + I_2(X, 11\leq\upsilon\leq24) \rightarrow O_2(X) + I_2(A')$	$10^{-12}\div10^{-11}$
102	$O_2(a,1) + I_2(X, \upsilon\geq15) \rightarrow O_2(X) + 2I$	10^{-11}
103	$O_2(a,2) + I_2(X, \upsilon\geq8) \rightarrow O_2(X) + 2I$	10^{-11}

[a] In the symbol $O_2(X,\upsilon)$ υ is the vibrational quantum number.

5. Spectroscopic detection of iodine oxides in the reactions of iodine with discharge excited oxygen

Kinetic modeling of EOIL systems suggests that the reaction set currently in use does not adequately reproduce the deactivation kinetics of I*. It appears that quenching by some as yet unidentified species is involved. We are exploring the possibility that IO_2 and higher oxides of iodine may be responsible for some of the quenching.

Cavity ring-down spectroscopy (CRDS) was used to observe iodine oxides formed in O_2/I_2 discharges. Fig. 7 shows a typical result from this experiment. This rotationally resolved band has been identified as the 2-9 $A^2\Pi_{3/2}$- $X^2\Pi_{3/2}$ transition of IO. The negative going trace in Fig. 7 is a simulation of the band based on the molecular constants of Durie et al. (Can. J. Phys. 38, 444 (1960)), with a rotational temperature of 40 K. Note that the lower vibrational level of this transition, v"=9, lies 5747 cm^{-1} above the zero-point energy. Hence, the observation of this transition indicates that vibrational relaxation in the jet was relatively inefficient.

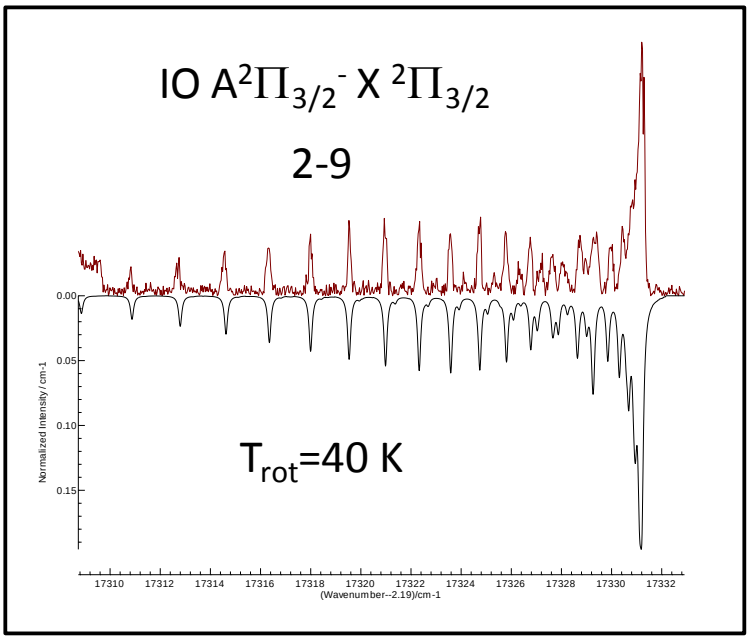

Figure 7. Observed and calculated spectra for IO

In addition to bands that could be assigned to known states of IO, there are several other bands where we have not yet identified the carrier or the transition type. Fig. 8 shows an example of one of the new features.

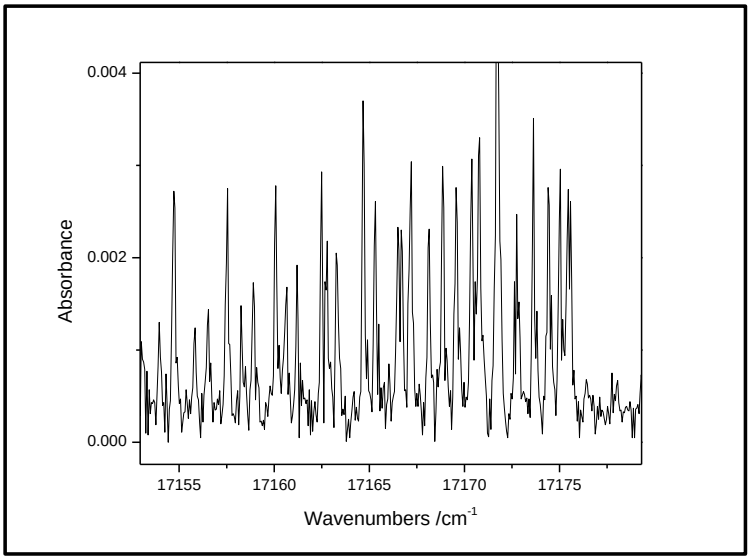

Figure 8. Rotationally resolved spectrum of an I_2/O_2 discharge product

The rotational line spacings in Fig. 8 indicate a relatively large rotational constant, comparable to that of IO(X). We are examining the possibility that the bands that show structure similar to that of Fig. 8 arise from the $A^2\Pi_{1/2}$- $X^2\Pi_{1/2}$ system of IO. The Ω=1/2 components of the A and X states have not been observed previously, and the spin-orbit coupling constants are unknown.

In addition to the features of IO and IO_2, several new band systems have been observed in the CRDS traces. An example of a low-resolution survey scan is show in Fig. 9. Further studies that include mass spectrometric detection are needed to identify the carriers of the unassigned bands.

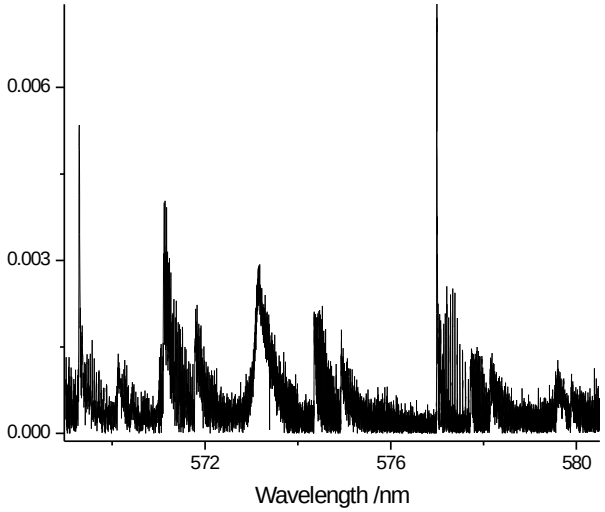

Figure 9. Absorption spectrum of the products from a discharge through a mixture of oxygen and iodine.

References

(1) A.D. Palla, D.L. Carroll, J.T. Verdeyen, W.C. Solomon, J. App. Phys. 100 (2006) 023117-11.

(2) A.D. Palla, J.W. Zimmerman, B.S. Woodard, D.L. Carroll, J.T. Verdeyen, T.C. Lim, W.C. Solomon, J. Phys. Chem. A 111 (2007) 6713-21.

(3) W.T. Rawlins, S. Lee, D.S. J., Proc. SPIE 6454-18 (2007).

(4) W.T. Rawlins, S. Lee, W.J. Kessler, S.J. Davis, App. Phys. Lett. 86 (2005) 051105.

(5) V.N. Azyazov, M.H. Kabir, I.O. Antonov, M.C. Heaven, J. Phys. Chem. A 111 (2007) 6592-99.

(6) V.N. Azyazov, I.O. Antonov, M.C. Heaven, J. Phys. Chem. A 111 (2007) 3010-15.

(7) O.V. Braginskiy, A.N. Vasilieva, K.S. Klopovskiy, A.S. Kovalev, D.V. Lopaev, O.V. Proshina, T.V. Rakhimova, A.T. Rakhimov, J. Phys. D: Appl. Phys. 38 (2005) 3609-25.

(8) A.-M. Diamy, J.-C. Legrand, V.V. Rybkin, S.A. Smirnov, Contrib. Plasma. Phys. 45 (2005) 5-21.

(9) J.T. Herron, D.S. Green, Plasma Chem. Plasma Proc. 21 (2001) 459.

(10) V. Jirasek, O. Spalek, J. Kodymova, M. Censky, Chem. Phys. 269 (2001) 167-78.

(11) I.A. Kossyi, A.Y. Kostinsky, A.A. Matveyev, V.P. Silakov, Plasma Sources Sci. Technol. 1 (1992) 207-20.

(12) R. Atkinson, D.L. Baulch, R.A. Cox, J.N. Crowley, R.F. Hampson, R.G. Hynes, M.E. Jenkin, M.J. Rossi, J. Troe, http://www.iupac-kinetic.ch.cam.ac.uk, 2006.

(13) D.S. Stafford, M.J. Kushner, J. Appl. Phys. 96 (2004) 2451.

(14) G.P. Perram, Int. J. Chem. Kin. 27 (1995) 817-28.

(15) O.V. Braginsky, A.S. Kovalev, D.V. Lopaev, O.V. Proshina, T.V. Rakhimova, A.T. Rakhimov, A.N. Vasilieva, J. Phys. D: Appl. Phys. 40 (2007) 6571-82.

(16) O.V. Braginsky, A.S. Kovalev, D.V. Lopaev, Y.A. Mankelevich, O.V. Proshina, T.V. Rakhimova, A.T. Rakhimov, A.N. Vasilieva, J. Phys. D: Appl. Phys. 39 (2006) 5183-90.

(17) G. Cartry, L. Magne, G. Cernogora, J. Phys. D: Appl. Phys. 32 (1999) L53-L56.

(18) M.J. Pinheiro, G. Gousset, A. Granier, C.M. Ferreira, Plasma Sources Sci. Technol. 7 (1998) 524-36.

(19) V.N. Azyazov, Kvantovaya Elektronika (Moscow) 21 (1994) 25-28.